Inorganic Chemistry

pubs.acs.org/IC Article

Electrochemical Exploration of Active Cu-Based Atom Transfer Radical Polymerization Catalysis through Ligand Modification

Jamie N. Melville and Paul V. Bernhardt*

Cite This: *Inorg. Chem.* 2021, 60, 9709–9719 Read Online

ACCESS | Metrics & More | Article Recommendations | Supporting Information

ABSTRACT: The intersection between Cu-catalyzed atom transfer radical polymerization (ATRP) and organometallic mediated radical polymerization (OMRP) has been recently shown to be a result of competition between the Cu^{I} and Cu^{II} complexes of polyamine ligands for the same organic free radical. The tetradentate ligands *N,N′*-bis-2′-pyridylmethyl-ethane-1,2-diamine (L^1) and *N,N′*-dimethyl-*N,N′*-bis-2′-pyridylmethyl-ethane-1,2-diamine (L^2) form stable Cu complexes which, depending on their oxidation state, can either liberate or complex organic radicals. Herein, we show that this process may be affected by subtle changes to the ligand system. Switching from a tertiary amine (L^2) to a secondary amine (L^1) retains ATRP and OMRP activity through a series of cyclic voltammetry measurements in the presence of the initiator bromoacetonitrile.

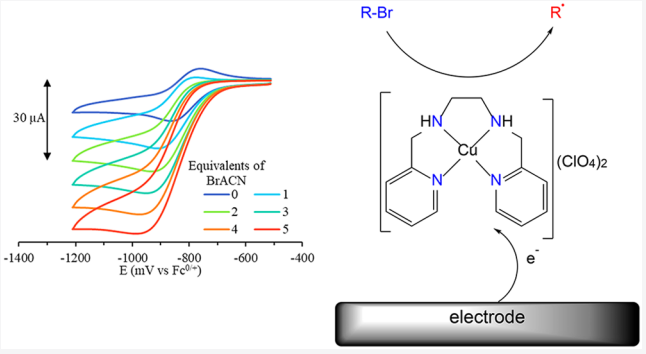

INTRODUCTION

Atom transfer radical polymerization (ATRP) is a controlled radical polymerization technique first demonstrated in 1995 in which the radical is generated via a reversible redox process that is mediated by a transition metal complex, in most cases containing copper, which cycles between its mono- and divalent forms.[1,2] As illustrated in Scheme 1, the initiating

Scheme 1. Cu-Catalyzed ATRP

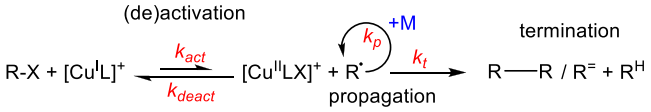

$$K_{ATRP} = \frac{[Cu^{II}LX][R^{\bullet}]}{[Cu^{I}L][R\text{-}X]} = \frac{k_{act}}{k_{deact}} \ll 1$$

catalyst $[Cu^{I}L]^+$ reacts reversibly with an alkyl halide (R–X) initiator, concurrently abstracting a halogen atom (X) (captured as $[Cu^{II}LX]^+$) and releasing a radical ($R^{\bullet}$). The radical adds to a monomer (M), and the polymer chain propagates (k_p) by consecutive reaction with other monomers. The radical activation process exists in dynamic equilibrium with the halide-terminated growing polymer chain.

The ATRP equilibrium constant, K_{ATRP} ($\ll 1$), limits the concentration of radicals to minimize radical–radical coupling (termination, k_t) reactions, and as such k_{act} must be smaller than k_{deact} by several orders of magnitude. However, k_{act} must still be large enough that the radical activation occurs at an appropriate rate.[3] Manipulation of these values is possible by varying the Cu catalyst, initiator, solvent, monomer, and/or halide involved in this equilibrium.

Copper is well suited to its role in ATRP catalysis. Upon oxidation from Cu^{I} to Cu^{II}, the coordination number rises from 4 to 5 (common for most Cu^{II} complexes).[4] This is necessary in ATRP systems, as halogen atom transfer to Cu^{I} requires an increase in coordination number. Copper complexes of multidentate N-donor ligands provide the most effective ATRP catalysts in terms of activity and stability of the complex in both oxidation states compared with ligands bearing O-, P-, or S-donors.[5] Essentially all of the Cu complexes used in ATRP comprise tertiary amine or pyridyl N-donors. The choice of ligand also governs the $Cu^{II/I}$ redox potential, and there is an empirical correlation between log K_{ATRP} and the $Cu^{II/I}$ redox potential (more negative potentials being associated with larger log K_{ATRP}).[6,7] Lower redox potentials also signal increasing stability of the Cu^{II} form of the catalyst relative to its Cu^{I} form.

Organic synthesis can be used to introduce inductive effects to the polyamine ligand that lower the $Cu^{II/I}$ redox potential. In 2018, Ribelli et al. synthesized a copper ATRP catalyst

Received: April 1, 2021
Published: June 18, 2021

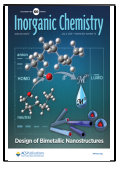

https://doi.org/10.1021/acs.inorgchem.1c01001
Inorg. Chem. 2021, 60, 9709–9719

based on tris-(2-pyridylmethyl)amine (TPMA), namely its 4-dimethylamino-substituted analog $TPMA^{NMe2}$.[8] The addition of electron-donating $-NMe_2$ groups to the pyridine rings of TPMA lowered the $Cu^{II/I}$ redox potential by more than 300 mV (from −240 mV to −554 mV vs SCE). This led to an increase of K_{ATRP} from $\sim10^{-5}$ (for $[Cu(TPMA)Br]^+$) to $\sim10^{-1}$ (for $[Cu(TPMA^{NMe2})Br]^+$) in MeCN, in the presence of the initiator methyl 2-bromoproprionate (MBrP).

Compared to tertiary polyamine ligands, which dominate ATRP Cu catalysis, their secondary amine analogs have received little attention.[9−11] This is important as a change to the N-donor (from a tertiary to a secondary amine) will lower the $Cu^{II/I}$ redox potential significantly as the Cu−N bonds shorten through relieved steric crowding.[12] This opens up the possibility for ATRP catalysts of even higher activity without the need for synthetic elaboration of the ligand system.

Herein, we study the Cu complexes of a homologous series of tetradentate N-donor ligands (Figure 1) based on the parent

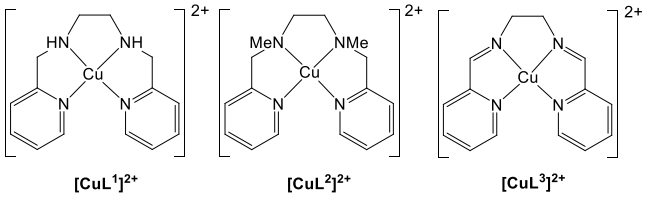

Figure 1. Three complexes studied in this work.

N,N′-bis(2-pyridylmethyl)ethylenediamine (L^1), and inclusive of its tertiary amine (L^2) and diimine (L^3) analogs. All three Cu complexes are known compounds, and their EPR and electronic spectroscopic properties have been investigated.[13−17] Crystal structures of two of these complexes, $[CuL^1]^{2+}$ and $[CuL^2]^{2+}$, are known,[15,18,19] and $[CuL^2]^{2+}$ has already found favor as an ATRP catalyst where it exhibits one of the highest activities of all Cu complexes.[20]

As many of the compounds relevant to ATRP are unstable (including the intermediate radicals and Cu^I complexes (Scheme 1)), mechanistic studies are not straightforward and we have developed novel electrochemical methods to generate these highly reactive intermediates *in situ* and understand their chemistry using combinations of time- and concentration-dependent voltammetry.[21−25] These studies have offered new ways to access kinetic information relevant to the use of these compounds in polymer chemistry.[26,27]

Recent research has revealed that, in some copper-mediated ATRP systems, organocopper(II) complexes may be formed by C-atom (radical) capture (as opposed to halogen atom transfer) to the Cu^I catalyst.[24,25,28] This intersects with organometallic mediated radical polymerization (OMRP) (Scheme 2),[29] a different controlled radical polymerization approach, and introduces a new layer of complexity that must be understood if fine control over activity is to be achieved in both ATRP and OMRP. Factors such as multidentate ligand structure, the radical, and the rate of deactivation all influence this balance, and this will be investigated in the present work by comparisons between the three homologues $[CuL^1]^{2+}$, $[CuL^2]^{2+}$, and $[CuL^3]^{2+}$.

Scheme 2. Competition between the Cu^I and Cu^{II} Forms of the Catalyst for the Radical R•

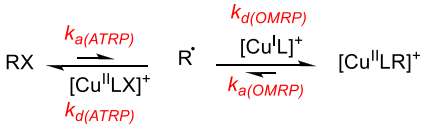

EXPERIMENTAL SECTION

Synthesis. *Safety Note.* Perchlorate salts are potentially explosive. Although no problems were encountered when handling the compounds in this work, they should not be heated in their solid state or scraped from sintered glass frits.

Reagents. Most solvents and reagents were obtained commercially and used without further purification. MeCN was distilled and dried over 3−4 Å molecular sieves prior to use.

$[CuL^1](ClO_4)_2$. A synthesis for L^1 has previously been reported (Figure 2), and this was followed with minor modifications.[18] A solution of pyridine-2-carbaldehyde (2.45 mL, 25.8 mmol) in MeOH (15 mL) and a solution of ethylenediamine (0.7 mL, 10 mmol) in MeOH (5 mL) were combined and refluxed, with stirring, for 3.5 h. After cooling to room temperature, $NaBH_4$ (1.6 g, 42 mmol) was added and the solution was stirred overnight. The solvent was removed via rotary evaporation to give a dark yellow oil. This was re-dissolved in water and extracted with four 50 mL aliquots of $CHCl_3$. The solvent was removed via rotary evaporation to give crude L^1 (2.6 g, approximately 10.7 mmol) as a brown oil. Some of this product (1.08 g, approximately 4.46 mmol) was dissolved in EtOH (10 mL). A solution of $Cu(ClO_4)_2·6H_2O$ (2.01 g, 5.42 mmol) in EtOH (15 mL) was added slowly with stirring. Water (15 mL) was added to prevent premature precipitation. The resulting mixture was stirred on gentle heat for 1 h before being purified on a Sephadex SP-25 (Na^+ form) column. A pale purple band eluted first with 0.3 M $NaClO_4$, followed by a light, bright blue band, and finally a major dark, vivid blue band of the desired compound. The dark blue solution was concentrated via rotary evaporation to one-quarter of its volume. Some purple precipitate formed on the sides of the flask. This was filtered off, and the filtrate was allowed to slowly concentrate at room temperature. After 10 d, deep blue/purple crystals formed (336 mg, 15%). Further crops could be obtained from the filtrate if desired. Anal. Calcd for $C_{14}H_{20}Cl_2CuN_4O_9$ (monohydrate 522.78 g mol^{-1}): C, 32.17; H, 3.86; N, 10.72. Found: C, 32.2; H, 3.62; N, 10.7. IR (cm^{-1}): 3249 (m, N−H, str), 3078 (w, ar. C−H str), 2969 (w, sat. C−H str), 1615 (m, C═C), 1452 (m, CH_2 bend), 1076 (s, Cl−O str). Visible absorption spectra λ_{max}/nm (ε/M^{-1} cm^{-1}): MeCN 599 (144); DMSO 621 (186). X-ray diffraction of the crystals matched the previously published structure of *rac*-$[CuL^1](ClO_4)_2$ (CCDC reference code IDUMEZ).[15]

$[CuL^2](ClO_4)_2$. A previously reported synthetic method for methylation of L^1 was followed with some modifications.[30] Crude L^1 (1.36 g, 5.61 mmol, prepared above) was dissolved in water (15 mL) and combined with CH_2O solution (8.0 mL, 37%) and HCOOH (7 mL, 99%). The mixture was refluxed, with stirring, for 3 d. Aqueous NaOH was added until the pH was approximately 13. The solution was extracted with four 40 mL aliquots of $CHCl_3$. The solvent was removed via rotary evaporation to give crude L^2 (1.4 g, 5.2 mmol). This product was dissolved in a minimal amount of MeOH (10 mL). A solution of $Cu(ClO_4)_2·6H_2O$ (2.01 g, 5.4 mmol) in MeOH (15 mL) was added slowly with stirring. The resulting mixture was stirred with warming for 3 h. Half of this mixture was purified on a Sephadex SP-25 (Na^+ form) column with 0.3 M $NaClO_4$ as the eluent. A minor pale purple band eluted first and was discarded. The desired product followed as an intensely blue band. This solution was concentrated via rotary evaporation to one-quarter of its volume. After 24 h, bright blue crystals (185 mg, 0.346 mmol) were collected. The remaining half of the reaction mixture (not purified by column chromatography) was left to concentrate for 3 d, which also afforded dark blue crystals identical to the fraction obtained after column chromatography (278 mg, 0.525 mmol). Overall, 463 mg (0.871 mmol, 17%) of $[CuL^2](ClO_4)_2$ were collected and further crops could be obtained from the filtrate if desired. Anal. Calcd for $C_{16}H_{22}Cl_2CuN_4O_8$ (532.82 g mol^{-1}): C, 36.07; H, 4.16; N, 10.52.

https://doi.org/10.1021/acs.inorgchem.1c01001
Inorg. Chem. 2021, 60, 9709−9719

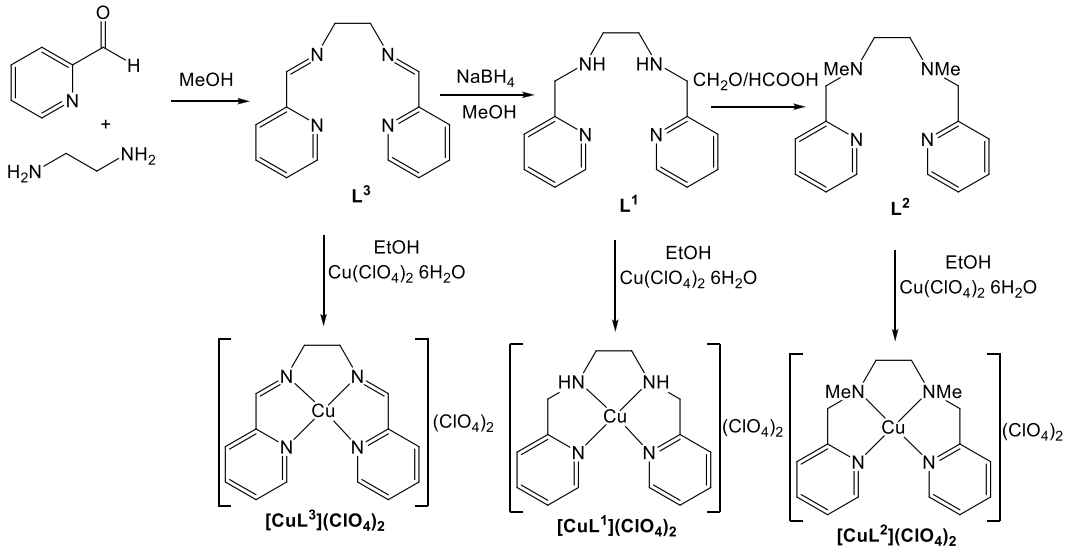

Figure 2. Synthetic summary of the compounds in this work.

Found: C, 35.9; H, 4.2; N, 10.2. IR (cm^{-1}, ATR): 2914 (w, sat. C−H str), 1614 (m, C═N str), 1447 (m, CH_2 bend), 1073 (s, Cl−O str). Visible absorption spectra λ_{max}/nm (ε/M^{-1} cm^{-1}): MeCN 623 (270); DMSO 642 (272). X-ray diffraction identified the complex as the known compound *meso*-$[CuL^2](ClO_4)_2$ (CCDC reference code IFIXUR).[19]

$[CuL^3](ClO_4)_2$. A solution of pyridine-2-carbaldehyde (4.42 g, 41.2 mmol) in MeOH (15 mL) and a solution of ethylenediamine (1.20 g, 20.0 mmol) in MeOH (5 mL) were combined and refluxed, with stirring, for 5.5 h. The solvent was removed via rotary evaporation to give a brown oil. This product was left under vacuum overnight to give crude L^3 (5.02 g, approximately 10 mmol). This product was dissolved in MeOH (35 mL), and a solution of $Cu(ClO_4)_2{\cdot}6H_2O$ (7.41 g, 20.0 mmol) dissolved in methanol (20 mL) was added dropwise. The resulting solution was stirred with gentle warming. After standing for 7 d at room temperature, small dark blue crystals of $[CuL^3](ClO_4)_2$ formed which were suitable for X-ray diffraction (5.81 g, 11.6 mmol, 58%). Anal. Calcd for $C_{14}H_{14}Cl_2CuN_4O_8$ (500.74 g mol^{-1}): C, 33.58; H, 2.82; N, 11.19. Found: C, 33.5; H, 3.0; N, 10.9. IR (cm^{-1}, ATR): 3074 and 3044 (ar. C−H str), 2969 and 2930 (w, sat. C−H str) 1663 (m, C═N str), 1604 (m, C═C str), 1046 (s, Cl−O str), 778 (s, ar. C−H bend). Visible absorption spectra λ_{max}/nm (ε/M^{-1} cm^{-1}): MeCN 612 (193); DMSO 628 (155).

PHYSICAL METHODS

UV−vis spectra were measured using a Shimadzu UV−2600 UV−visible spectrophotometer over the range 300−900 nm. Solid state IR spectroscopy was performed on a PerkinElmer Frontier FTIR spectrometer from 4000 to 550 cm^{-1} in Attenuated Total Reflectance mode. Elemental microanalyses were acquired on a FLASH 2000 CHNS/O Analyzer.

Cyclic voltammetry was performed using a BAS100B/W potentiostat, a glassy carbon working electrode (surface area = 0.055 cm^2), platinum counter electrode, and non-aqueous Ag/Ag^+ reference electrode in either DMSO or MeCN with 0.1 M $(Et_4N)ClO_4$ supporting electrolyte. Ferrocene was used as an external standard, and all potentials were cited versus $Fc^{+/0}$. All solutions were purged with nitrogen prior to each measurement. Following each measurement, the working electrode was polished using 0.05 μm alumina nanoparticles, rinsed with water and acetone, and dried. Voltammetry data were simulated with the program Digisim,[31] and the simulation parameters (rate coefficients, redox potentials, diffusion coefficients, etc.) are summarized in Table 2 and Table S1.

UV−visible Spectrophotometric Titrations. In a standard titration, 0.1 equiv of bromide (as 200 mM $(Et_4N)Br$ solutions in either DMSO or MeCN) was added to 2 mL of a 3.0 mM solution of $[CuL^n]^{2+}$ (n = 1, 2, 3) in the same solvent. The complex solution also contained 0.1 M $(Et_4N)ClO_4$ as the supporting electrolyte to mirror the conditions of subsequent cyclic voltammetry experiments. Aliquots of bromide solution were added past the stoichiometric end point (1:1) complex to ensure complete formation of the bromido complex. Once the spectra exhibited no further changes with successive bromide additions, the titration was finished. Global analysis of the data collected was undertaken using ReactLab EQUILIBRIA[32] to obtain the requisite bromide binding constants ($K_{II,Br}$) (Scheme 3).

Scheme 3. Model Describing Cu-Catalyzed Electrochemical Radical Activation and Deactivation by Atom Transfer

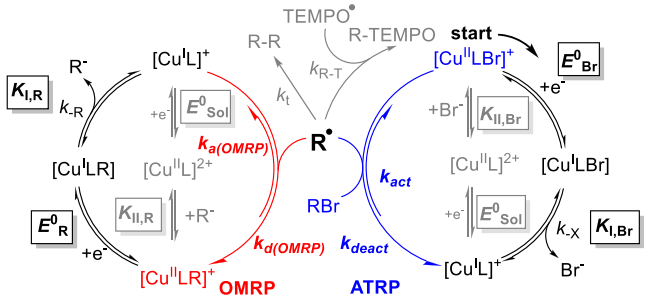

X-ray Crystallography. X-ray crystallographic data were collected at 190 K on an Oxford Diffraction Gemini diffractometer operating within the range $2 < 2\theta < 50°$ with Mo Kα radiation (λ = 0.71073 Å). The structure was solved and refined with SHELX.[33] Calculations were all undertaken within the WinGX program.[34] Images of all structures were created in Mercury.[35] Data in CIF format have been deposited with the CCDC (2074222).

RESULTS AND DISCUSSION

Structural, Spectroscopic, and Electrochemical Characterization. *Structural Considerations.* Crystalline samples of $[CuL^1](ClO_4)_2$, $[CuL^2](ClO_4)_2$, and $[CuL^3](ClO_4)_2$ were obtained and used in all experiments. The structure of $[CuL^3](ClO_4)_2$ is new. The complex occupies a crystallographic two-fold axis (Figure 3). The copper has a distinctively flat CuN_4 plane as part of a tetragonally elongated octahedral geometry, enforced by the rigidity of the numerous double bonds within the ligand structure. This forces the hydrogens

https://doi.org/10.1021/acs.inorgchem.1c01001
Inorg. Chem. 2021, 60, 9709−9719

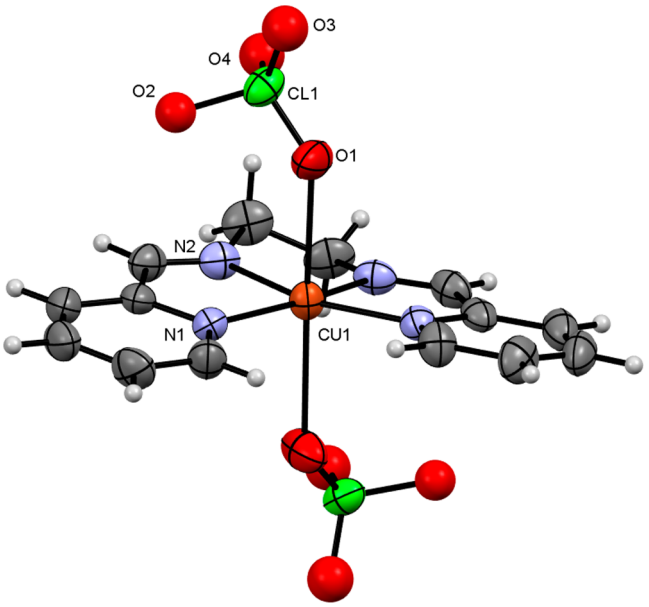

Figure 3. View of the crystal structure of $[CuL^3](ClO_4)_2$ (30% probability ellipsoids). Perchlorate disorder omitted for clarity. Selected bond lengths and angles: Cu1−N1 2.007(4), Cu1−N2 1.953(4), Cu1−O1 2.517(3) Å; N2−Cu1−N1 82.0(2), N2−Cu1−N2′ 82.0(2)°.

on the two methylene carbon atoms into an eclipsed formation, introducing a source of torsional strain to the C−C bond. The weakly bound axial perchlorate ligands are a consequence of an underlying Jahn−Teller distortion of the otherwise degenerate ^2E_g electronic ground state. Any ligands bound in the equatorial plane will exhibit shorter bond lengths to the metal than ligands aligned with the d_{z^2} orbital.

There are several known crystal structures of L^3 bound as a tetradentate ligand to transition metals,[36] lanthanoid ions,[37] and main group metals,[38] but, interestingly, a large proportion of them involve the ligand binding to two metals in a bridging bis-bidentate mode.[39−41] This includes the dicopper(I) complexes $[Cu_2(L^3)_2]^{2+}$ (a double helicate structure)[42] as well as the non-helical $[(Ph_3P)ICu(L^3)CuI(PPh_3)]$[43] and $[(Ph_3P)_2Cu(L^3)Cu(PPh_3)_2]^{2+}$ complexes.[44]

Crystallographic analysis of $[CuL^1](ClO_4)_2$ and $[CuL^2](ClO_4)_2$ revealed them to be identical to their previously published structures,[15,18,19] and the crystal structures of $[CuL^1](ClO_4)_2$, $[CuL^2](ClO_4)_2$, and $[CuL^3](ClO_4)_2$ are compared in Figure 4. Despite their apparent similarity, they exhibit quite different coordination geometries and physical properties (Table 1) due to stereochemical changes at the ethylenediamine/diimine N-donors (N2 in Figure 3). Without the C═N(2) double bond present in $[CuL^3]^{2+}$, the ligands in $[CuL^1](ClO_4)_2$ and $[CuL^2](ClO_4)_2$ are able to fold away from planarity, relieving the torsional strain on the central C−C bond. This also introduces stereogenic centers at each NH/NMe donor, meaning that two N-based isomers of these complexes may exist; *rac*, with the hydrogen/methyl substituents on N2 on opposite sides of the CuN_4 plane, and *meso*, where they occupy the same side. Crystalline $[CuL^1](ClO_4)_2$ prepared herein (Figure 4A) corresponds to the *rac* isomer.[15] Conversely, crystals of $[CuL^2](ClO_4)_2$ are the *meso* isomer (Figure 4B).[19]

The geometrical distortion from CuN_4 planarity is most pronounced in the structure of $[CuL^2](ClO_4)_2$. This distortion is enforced by the addition of a methyl group to each N which causes crowding of the CuN_4 plane. If one of the weakly bound perchlorate ions is treated as a fifth ligand, as Pandiyan et al.[19] have in their analysis, the divergence of the CuN_4 group from planarity can be quantified using the τ_5 parameter (eq 1) for 5-coordinate metal complexes:[45]

$$\tau_5 = \frac{\beta - \alpha}{60^o} \quad (1)$$

where $\beta > \alpha$ are the two largest coordinate angles. The τ_5 parameter was intended to fall between 0 and 1, with 0 being ideal square pyramidal and 1 perfect trigonal bipyramidal, although it has been pointed out that τ_5 may be greater than 1.[46,47] The τ_5 values for each of the three complexes are shown in Figure 4. This illustrates the significant structural change enacted upon the coordination center by hydrogenation and then methylation of N2 as well as the stereochemistry at the amine N-donor.

Few perfectly trigonal bipyramidal or square pyramidal Cu^{II} structures are known. Indeed, crystal structures of several Cu complexes of L^1 and L^2 with various coligands are known and all show some degree of distortion.[48−54] The Supporting Information shows a selection of these (Figure S1), to enable a better understanding of the extent to which divergences from ideal 5-coordinate geometries (trigonal bipyramidal and square pyramidal) are common among complexes of this type. The *rac*-$[CuL^1]^{2+}$ isomer is dominant for structures of this complex, but for $[CuL^2]^{2+}$ there are approximately equal numbers of *meso* and *rac* isomers. It is apparent that the *rac* isomers of $[CuL^2]^{2+}$ adopt distinctly folded (non-planar) conformations, and the two pyridyl groups occupy *trans* coordination sites in some extreme cases. The only Cu^I structure of these ligands is *rac*-$[CuL^2]BF_4$ (CCDC reference code AXOKUV[48]) which

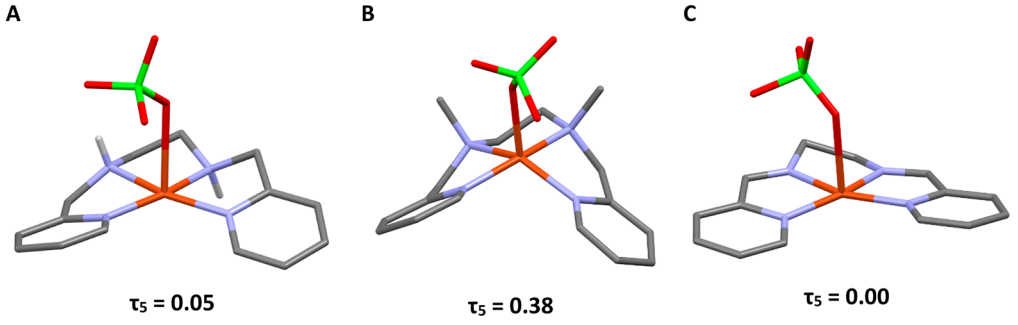

Figure 4. Crystal structures of (A) *rac*-$[CuL^1](ClO_4)_2$ (IDUMEZ[15]), (B) *meso*-$[CuL^2](ClO_4)_2$ (IFIXUR[19]), and (C) $[CuL^3](ClO_4)_2$ (this work). Only one ClO_4^- shown for comparison and C−H atoms are omitted for clarity. The distortion parameter τ_5 is shown for each structure.

https://doi.org/10.1021/acs.inorgchem.1c01001
Inorg. Chem. 2021, 60, 9709−9719

Table 1. Spectroscopic, Thermodynamic, and Electrochemical Data for $[CuL^n]^{2+}$ (n = 1, 2, 3) and Their Bromido Complexes in MeCN and DMSO

	MeCN			DMSO		
	λ_{max}/nm (ε/M^{-1} cm^{-1})	log K_{IIBr}	$E(Cu^{II/I})$/mV vs $Fc^{+/0}$	λ_{max}/nm (ε/M^{-1} cm^{-1})	log K_{IIBr}	$E(Cu^{II/I})$/mV vs $Fc^{+/0}$
$[CuL^1]^{2+}$	599 (144)	–	−634	621 (186)	–	−764
$[CuL^1Br]^{+}$	688 (190)	5.05(5)	−784	688 (240)	3.109(1)	−814
$[CuL^2]^{2+}$	623 (270)	–	−547	642 (166)	–	−649
$[CuL^2Br]^{+}$	784 (272)	>5	−697	737 (209)	3.291(1)	−699
$[CuL^3]^{2+}$	612 (193)	–	−129	628 (155)	–	−243
$[CuL^3Br]^{+}$	751 (269)	3.381(8)	−352	695 (174)	3.756(5)	−260

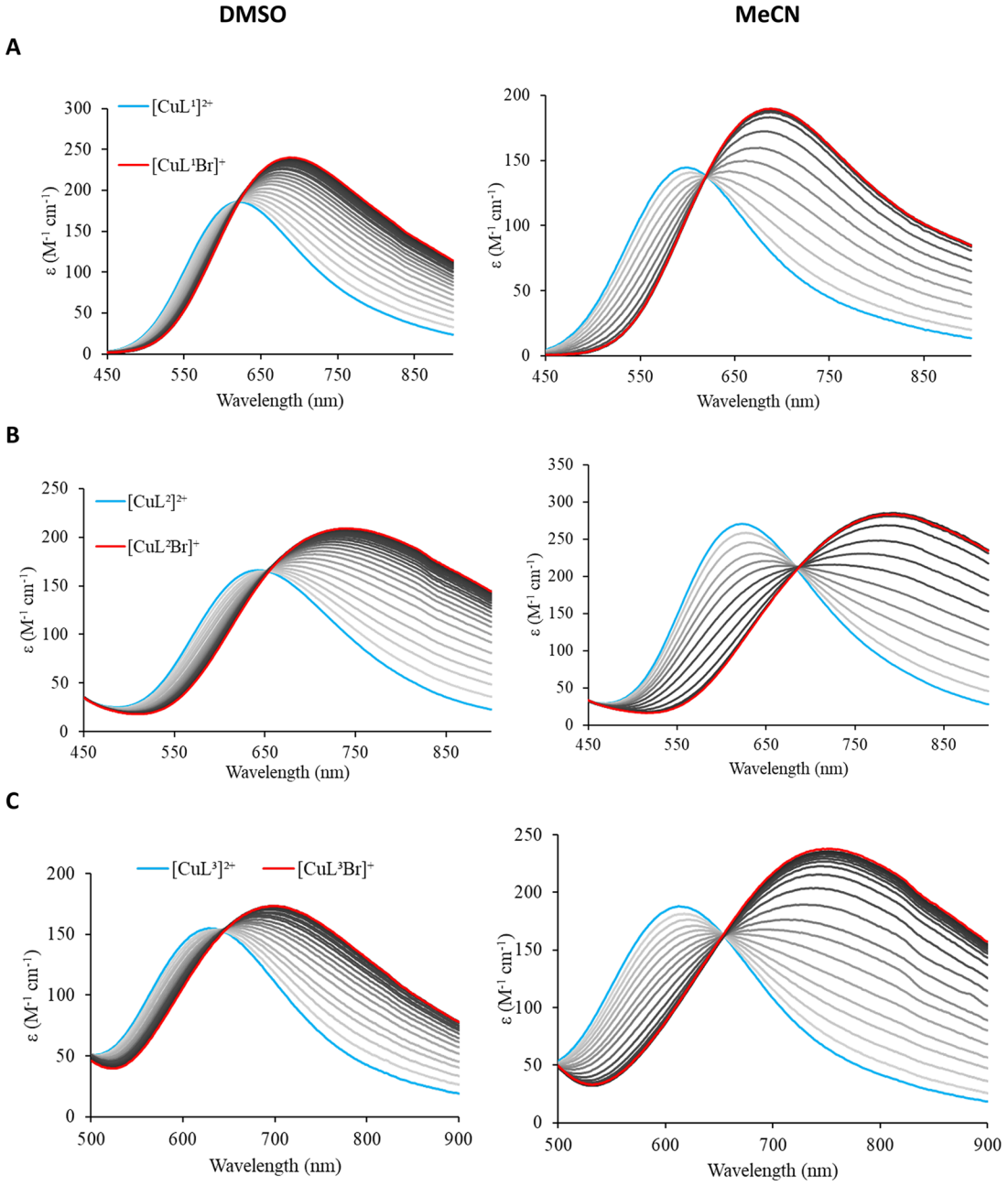

Figure 5. Visible absorption spectra upon sequential addition of bromide to (**A**) $[CuL^1]^{2+}$, (**B**) $[CuL^2]^{2+}$, and (**C**) $[CuL^3]^{2+}$ in DMSO (left) and MeCN (right).

also shows a folded conformation of the 4-coordinate complex as would be expected for an ideally tetrahedral monovalent Cu compound.

Bromide Affinity. As the product of ATRP radical activation, the halide (in this case bromide) binding constant of the resulting Cu^{II} complex is an important component of

https://doi.org/10.1021/acs.inorgchem.1c01001
Inorg. Chem. 2021, 60, 9709−9719

any prospective catalyst. UV−vis spectrophotometric titrations of $[CuL^n]^{2+}$ (n = 1, 2, 3) with bromide were carried out in both MeCN and DMSO. The data from these titrations were analyzed using ReactLab EQUILIBRIA[32] to determine the bromide binding constants ($K_{II,Br}$) in each solvent. Additionally, analysis of the resultant spectra gives valuable information about the structure of these complexes in solution, in an environment as close as possible to that in which the ATRP reaction would take place. The data are summarized in Table 1.

The spectral changes upon bromide addition for the three complexes in MeCN and DMSO (Figure 5) are rather similar. Clear isosbestic points are seen which indicates that only two absorbing species are ever present. The perchlorate anion is a notoriously poor ligand and in solution does not compete with the solvent for coordination sites on labile metal ions such as Cu^{II}. Therefore, the initial complexes shown as $[CuL^n]^{2+}$ in Figure 5 are best represented as $[CuL^n(solv)]^{2+}$ (solv = MeCN or DMSO), which explains the bathochromic shifts in peak maxima going from MeCN (an N-donor) to DMSO (an O-donor).

The electronic maxima (Table 1) are all of d−d origin for the d^9 electronic configuration, and this peak varied according to the donor strength of the fifth ligand (solvent or bromide). In all cases, the absorption peaks exhibited a bathochromic and hyperchromic shift over the course of the bromide titration (see Table 1). This is consistent with coordination of the weak field bromide ion in place of the previously N- or O-bound solvent. Typically, this change was accompanied by broadening and increased asymmetry of the peak which is indicative of a less symmetric ligand field. Notably, the crystal structure of *rac*-$[CuL^1Cl]^+$ finds the chlorido ligand tightly bound in the equatorial CuN_3 plane while one pyridyl ligand is weakly bound in the axial site (CCDC reference code CPAZHC, Figure S1).[50] Folding of the ligand results in a τ_5 value of 0.14, compared with *rac*-$[CuL^1](ClO_4)_2$ (0.02). Also, this conformational change may occur with retention of the *rac* N-based isomeric configuration as the pyridyl group switches from equatorial to axial.

On the basis of existing crystallographic data, it appears that the *meso*-$[CuL^2]^{2+}$ isomer (identified here as *meso*-$[CuL^2](ClO_4)_2$) prefers to accommodate additional coligands in an axial coordination site as seen in *meso*-$[CuL^2(NCMe)]^{2+}$ and *meso*-$[CuL^2Cl]^+$ (Supporting Information Figure S1).[48,51] On the other hand, *rac*-$[CuL^1]^{2+}$ may fold without N-inversion and the incoming ligand can bind in the equatorial plane as in *rac*-$[CuL^1Cl]^+$.[50]

The bromide binding constant for each complex ($K_{II,Br}$) was determined, or estimated, in both MeCN and DMSO by global analysis of the spectrophotometric bromide titration using ReactLab EQUILIBRIA.[32] Although the bathochromic shifts in peak maxima in Figure 5 are similar, a more in-depth analysis of these spectral changes as a function of concentration (Supporting Information Figure S2) reveals that the bromide titrations of $[CuL^1]^{2+}$ and $[CuL^2]^{2+}$ in MeCN are associated with *sharp* end points corresponding to a stoichiometric equivalent of bromide. This means that their calculated bromide constants are only lower bounds (log $K_{II,Br}$ > 5) while those obtained in DMSO, where spectral changes approach a plateau asymptotically, lead to lower and better-defined bromide binding constants. The outlier is $[CuL^3(solv)]^{2+}$, which showed similar bromide binding constants in DMSO to $[CuL^1]^{2+}$ and $[CuL^2]^{2+}$, but a much lower formation constant in MeCN.

Cyclic Voltammetry. The redox potentials of all components within Scheme 3 were obtained from their CVs (Figure 6), and their values appear in Table 1. The $Cu^{II/I}$ redox

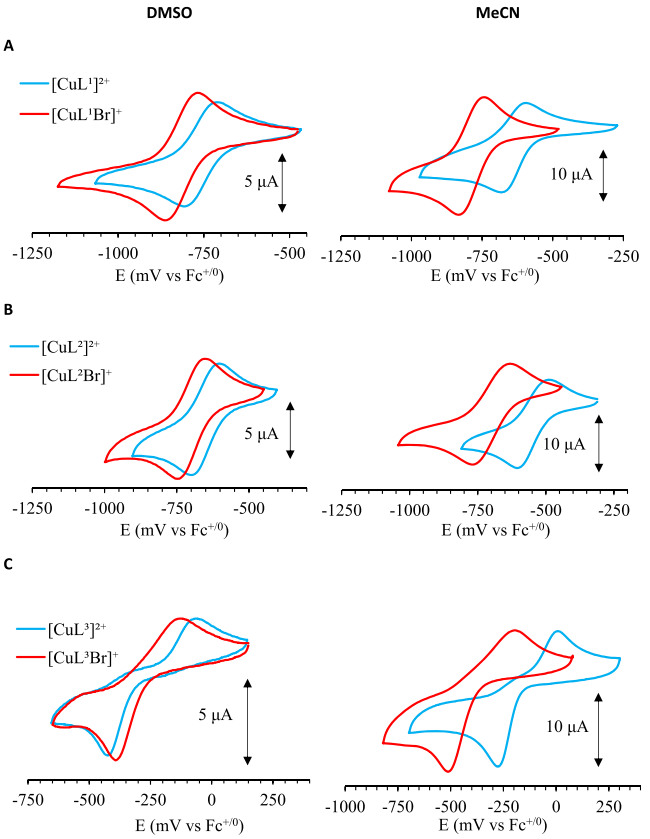

Figure 6. CVs of the complexes in this work with and without bromide (A) $[CuL^1]^{2+}$, (B) $[CuL^2]^{2+}$, and (C) $[CuL^3]^{2+}$. All complexes 1 mM with 0.1 M $(Et_4N)ClO_4$ and the scan rate is 50 mV s^{-1}. The systems in DMSO are on the left and those in MeCN are on the right.

potentials of the $[CuL^n]^{2+}$ (n = 1, 2, 3) complexes (E_L) were of the species $[CuL^n(solv)]^{2+}$ (solv = MeCN or DMSO). Addition of excess $(Et_4N)Br$ produced the $[CuL^nBr]^+$ complexes *in situ* (on the basis of their bromide binding constants, Table 1) and allowed their redox potentials (E_{LBr}) to be determined similarly. For $[CuL^1]^{2+}$ and $[CuL^2]^{2+}$ (and their bromido complexes, Figure 6A and 6B) the $Cu^{II/I}$ CV responses were symmetrical and quasi-reversible in MeCN and DMSO, which suggests minimal rearrangement of their coordination spheres upon reduction (apart from the expected change in coordination number from 5 (Cu^{II}) to 4 (Cu^{I}) which can be accommodated by reversible dissociation of one donor atom).[4]

For $[CuL^3]^{2+}$ and $[CuL^3Br]^+$ (Figure 6C) the CVs were asymmetric and irreversible, and the estimated redox potentials were more than 300 mV positive of the $[CuL^1]^{2+}$ and $[CuL^2]^{2+}$ analogs in both MeCN and DMSO. With increasing scan rates, the CV responses become more distorted (Figure S2) which is indicative of slow heterogeneous electron transfer. Rigidity of the tetradentate diimine chelating ligand and its preference for a planar geometry are evidently also unsuitable for Cu^{I}, and significant structural rearrangement occurs after reduction of

https://doi.org/10.1021/acs.inorgchem.1c01001
Inorg. Chem. 2021, 60, 9709−9719

Table 2. Values of k_{act}, k_{deact}, K_{ATRP}, $k_{a(OMRP)}$, $k_{d(OMRP)}$, and K_{OMRP} for $[CuL^1Br]^+$ and $[CuL^2Br]^+$ in MeCN and DMSO, with either BrACN or EBriB Initiators

		BrACN			EBriB		
		k_{act} (M^{-1} s^{-1})	k_{deact} (M^{-1} s^{-1})	K_{ATRP}	k_{act} (M^{-1} s^{-1})	k_{deact} ($M^{-1}s^{-1}$)	K_{ATRP}
$[CuL^1Br]^+$	MeCN	3.0×10^3	6.0×10^5	5.0×10^{-3}	1.0×10^3	1.4×10^5	7.0×10^{-3}
	DMSO	5.0×10^3	1.6×10^7	3.1×10^{-4}	2.5×10^3	6.8×10^6	5.9×10^{-4}
$[CuL^2Br]^+$	MeCN	1.4×10^3	1.7×10^5	8.0×10^{-3}	1.4×10^3	4.6×10^5	2.9×10^{-3}
	DMSO	1.2×10^3	2.4×10^6	5.0×10^{-4}	4.0×10^3	1.6×10^6	2.5×10^{-3}
		BrACN			EBriB		
		$k_{a(OMRP)}$ (s^{-1})	$k_{d(OMRP)}$ (M^{-1} s^{-1})	K_{OMRP} (M^{-1})			
$[CuL^1Br]^+$	MeCN	5.9×10^1	4.9×10^7	8.3×10^6	No OMRP activity detected		
	DMSO	3.0×10^{-1}	1.5×10^6	9.4×10^6			
$[CuL^2Br]^+$	MeCN	2.4×10^0	1.3×10^8	5.4×10^7			
	DMSO	2.2×10^{-1}	8.7×10^6	3.8×10^7			

$[CuL^3]^{2+}$ to produce a Cu^I complex that is reoxidized at a different potential.

The complete set of parameters describing the voltammetry of $[CuL^n]^{2+}$ and $[CuL^nBr]^+$ (n = 1,2) in both MeCN and DMSO is assembled in the Supporting Information (Table S1). The redox potentials of the bromido complexes were lower than the solvent complexes, typically by 50−150 mV. This is expected following the addition of the anionic bromide. The redox potentials of the CuL^1/Br complexes were 60 to 100 mV more negative than the Cu/L^2/Br analogs depending on the solvent. This is expected for copper complexes containing secondary amines instead of tertiary amines[12] and attributable to steric effects that elongate the Cu−N bonds of the tertiary amine complex and stabilize the larger Cu^I ion.

The negative shift in $Cu^{II/I}$ redox potential upon bromide replacing the solvent ligand ($E_{sol}^0 - E_{Br}^0$) for both $[CuL^1]^{2+}$ and $[CuL^2]^{2+}$ was markedly greater in MeCN than in DMSO (see Figure 6A and 6B). The shape of the CV waveform was unchanged between the solvent and bromido complexes, with very similar peak to peak separations and comparable anodic to cathodic current ratios. The magnitude of this shift in redox potential upon bromide coordination is related to the corresponding bromide binding constants of the Cu^{II} and Cu^I complexes by eq 2:

$$E_{sol}^0 - E_{Br}^0 = 59.2 \log \frac{K_{II,Br}}{K_{I,Br}} \quad (2)$$

Equation 2 then enables the Cu^I bromide formation constants to be calculated from the CV data and the spectrophotometric bromide titration data on the Cu^{II} analogs (Table 1). A key point is that the smaller shift of potential in DMSO leads to a stronger Cu^I bromido complex relative to MeCN, where the Cu^I−Br bond is destabilized to a greater degree.

Kinetics of Radical Activation and Deactivation. The methodology that we have developed for using cyclic voltammetry to extract kinetic information from ATRP activation and deactivation has been described elsewhere.[21,23,24] A key advantage of the technique is that stable Cu^{II} precursor complexes may be prepared, which are then converted electrochemically into their active Cu^I form *in situ*. The ensuing coupled chemical reactions with this Cu^I complex are bimolecular, and their rates can be tuned by concentration-dependent experiments. Within the electrochemical system, the voltammetry scan rate is also a critical variable, as it allows different time scales to be selected (all other things being equal), which can either actuate or preclude coupled chemical reactions depending on their rate constant. Reproducing the experimental CV data by simulation, using the model in Scheme 3, allows the key rate constants in this system to be obtained.

A typical cyclic voltammetry experiment consisted of the sequential addition of 1 equiv aliquots of alkyl halide initiator to a 5.0 mL DMSO or MeCN solution containing 1.0 mM $[CuL^n]^{2+}$ (n = 1, 2, 3), 2.0−4.0 mM $(Et_4N)Br$, 0.1 M $(Et_4N)ClO_4$ and, in half of the experiments, 0.05 M TEMPO as a radical scavenger. Sweep−rate dependent voltammetry (50 mV s^{-1}, 100 mV s^{-1}, 200 mV s^{-1}, 500 mV s^{-1}, and 1000 mV s^{-1}) was measured for each initiator concentration and for the starting solution.

Upon electrochemical reduction of the starting complex $[Cu^{II}LBr]^+$ (eq 3), reaction with the initiator RBr (radical activation, eq 4 rate constant k_{act}) is rate-limiting and irreversible in the presence of the nitroxyl radical trap 2,2,6,6-tetramethylpiperidine-1-oxyl (TEMPO, eq 5). The combination of eqs 3 and 4 constitutes an EC_{cat} mechanism where the coupled radical activation reaction regenerates the initial complex $[Cu^{II}LBr]^+$ and a catalytically enhanced cathodic current emerges.

$$[Cu^{II}LBr]^+ + e^- \rightarrow [Cu^{I}L]^+ + Br^- \quad (3)$$

$$[Cu^{I}L]^+ + RBr \leftrightarrows [Cu^{II}LBr]^+ + R^{\cdot}\ k_{act}/k_{deact} \quad (4)$$

$$R^{\cdot} + TEMPO^{\cdot} \rightarrow R\text{-}TEMPO \quad (5)$$

Accurate values of k_{act} are obtained by simulating the CV data taken at different sweep rates and RBr concentrations using the program Digisim.[31] The reverse reaction rate of eq 4 (k_{deact}, radical deactivation and see Scheme 3) can then be determined in a similar manner when TEMPO is omitted as eq 5 vanishes and eq 4 becomes reversible. The decrease in catalytic current (eq 3) is due to radical deactivation (k_{deact}).

In cases where OMRP activity (Scheme 3, left-hand side) occurs[24] concurrently with ATRP (Scheme 3, right-hand side), a redox response for the organometallic species, $[Cu^{II/I}LR]^{+/0}$, appears as a second wave (E_R), typically at a lower potential than E_{Br}. Other parameters pertinent to the system ($k_{a(OMRP)}$, $k_{d(OMRP)}$) are also found by simulation.[24,25] Simulations across the full range of initiator concentrations and sweep rates were carried out to determine K_{ATRP} (= k_{act}/k_{deact}), $K_{I,Br}$, E_{sol}, E_{Br}, and, where applicable, K_{OMRP}, $k_{a(OMRP)}$, $k_{d(OMRP)}$, and E_R. Note that in Scheme 3 some of the equilibrium constants and redox

https://doi.org/10.1021/acs.inorgchem.1c01001
Inorg. Chem. 2021, 60, 9709−9719

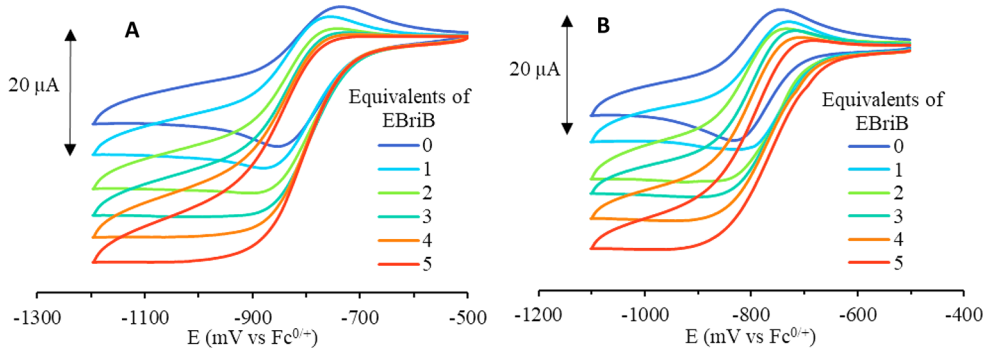

Figure 7. CVs of the sequential addition of 1 equiv aliquots of EBriB to 1 mM $[CuL^1Br]^+$ in MeCN (A) with and (B) without 0.05 M TEMPO. Both solutions contained 0.1 M $(Et_4N)ClO_4$ as supporting electrolyte. Scan rate: 50 mV s^{-1}.

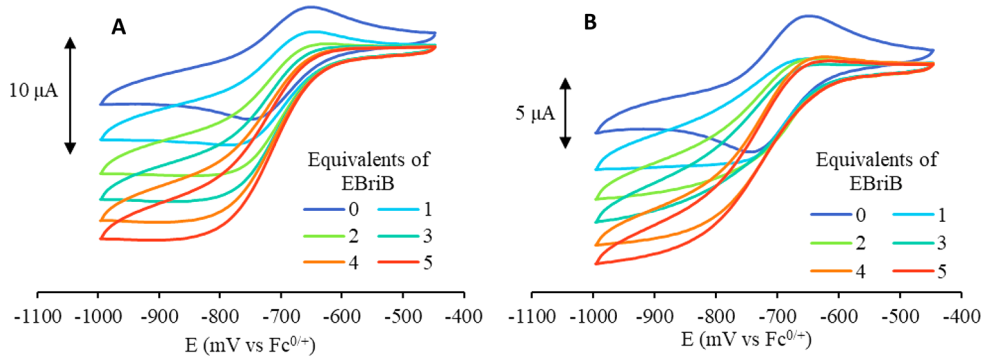

Figure 8. CV of the sequential addition of 1 equiv aliquots of EBriB to 5.0 mL of 1 mM $[CuL^2Br]^+$ in DMSO (A) with and (B) without (right) 0.05 M TEMPO. Both solutions contained 0.1 M $(Et_4N)ClO_4$ as supporting electrolyte. Scan rate: 50 mV s^{-1}.

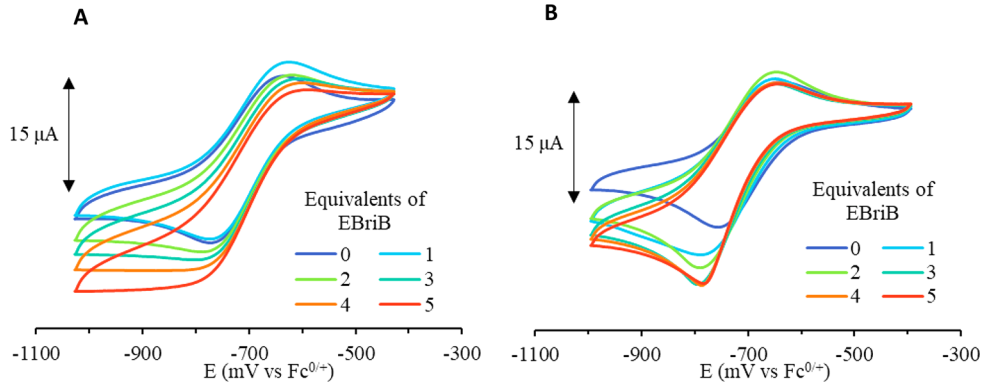

Figure 9. CV of the sequential addition of 1 equiv aliquots of EBriB to 5.0 mL of 1 mM $[CuL^2Br]^+$ in MeCN (A) with and (B) without 0.05 M TEMPO. Both solutions contained 0.1 M $(Et_4N)ClO_4$ as supporting electrolyte. Scan rate: 50 mV s^{-1}.

potentials are interdependent, as this is a closed thermodynamic cycle (see eq 2).

Two alkyl bromide initiators, ethyl bromoisobutyrate (EBriB) and bromoacetonitrile (BrACN), were titrated into electrochemical solutions containing the divalent $[CuL^nBr]^+$ (n = 1, 2) complexes and supporting electrolyte. All rate constants determined by this method are assembled in Table 2. Figures 7−10 show examples of the catalytic voltammetry, and representative experimental and simulated CVs are given in the Supporting Information (Figures S4−S11). Briefly, $[CuL^3Br]^+$ was found to be inactive as a catalyst in either MeCN or DMSO, and additions of EBriB or BrACN elicited no detectable changes in the CV. The inactivity of this complex was likely due to its higher redox potentials and irreversible electron transfer behavior.

Electrocatalytic Activity of $[CuL^nBr]^+$ with EBriB. An example of catalytic radical activation of EBriB by $[CuL^1Br]^+$ (electrochemically reduced to $[CuL^1]^+$) is shown in Figure 7. An enhancement of the current in the vicinity of the $[CuL^1Br]^{+/0}$ couple is apparent upon sequential addition of EBriB, along with a loss of the anodic peak as all $[CuL^1]^+$ is consumed by EBriB before it can be electrochemically reoxidized. The slightly diminished cathodic current in the absence of TEMPO (Figure 7B) illustrates the effect of the deactivation reaction on partially depleting $[CuL^1Br]^+$ at the electrode surface.

Similar behavior is seen with $[CuL^2Br]^+$. A single catalytic current response is seen at the $[CuL^2Br]^{+/0}$ potential, which is ca. 100 mV more positive than $[CuL^1Br]^{+/0}$ (Figure 8, data in DMSO).

https://doi.org/10.1021/acs.inorgchem.1c01001
Inorg. Chem. 2021, 60, 9709−9719

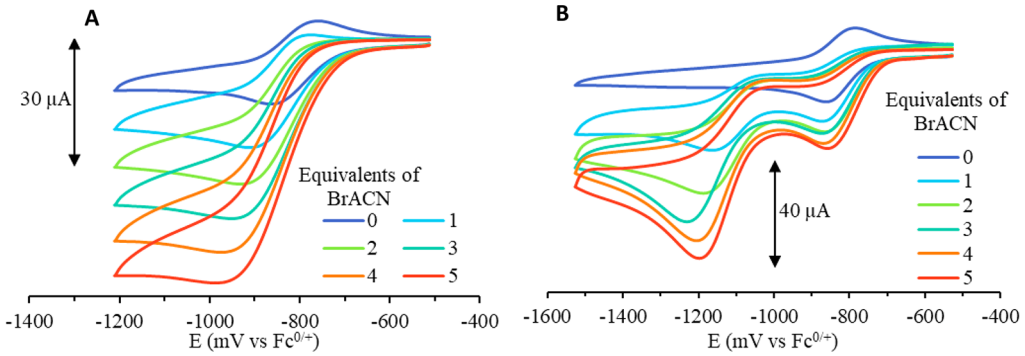

Figure 10. CVs of the sequential addition of 1 equiv aliquots of BrACN to 5.0 mL of 1 mM $[CuL^1Br]^+$ in MeCN (A) with and (B) without 0.05 M TEMPO. Both solutions contained 0.1 M $(Et_4N)ClO_4$ as supporting electrolyte. Scan rate: 50 mV s^{-1}.

An interesting feature of the $[CuL^2Br]^+$/EBriB voltammetry in MeCN (Figure 9B), when compared with the same system in DMSO (Figure 8B), was the relative insensitivity of the CV to EBriB addition (in the absence of TEMPO). Increases in the cathodic current were very small, and the anodic peak current persisted with successive additions of EBriB. With TEMPO present, this peculiarity abates, with a more sigmoidal waveform found after 5 equiv of EBriB when TEMPO is present (Figure 9A).

Electrocatalytic Activity of $[CuL^nBr]^+$ with BrACN. When BrACN was introduced to a solution of $[CuL^1Br]^+$ (in the absence of TEMPO), CVs comprising two separate redox responses were observed; one from $[CuL^1Br]^{+/0}$ at higher potential and one from the organocopper(II) complex $[CuL^1(CH_2CN)]^{+/0}$ (Figure 10B). In the presence of TEMPO (Figure 10A), only the higher potential catalytic response is seen, which indicates that the lower potential couple is a product of a reaction involving the radical $NCCH_2^\bullet$ that is otherwise quenched by TEMPO. This mirrors our previous observations using BrACN as an initiator.[24,25] Recently, Matyjaszewski et al. reported similar behavior with different complexes using this methodology.[26] The organocopper complex $[CuL^1(CH_2CN)]^+$ forms by rapid capture of the radical $NCCH_2^\bullet$ by $[CuL^1]^+$ within the reaction layer at the electrode surface, which is a demonstration of the OMRP deactivation reaction ($k_{d(OMRP)}$). The Supporting Information shows the corresponding CVs of $[CuL^1Br]^+$/BrACN in DMSO (Figure S7), $[CuL^2Br]^+$/BrACN in MeCN (Figure S9), and $[CuL^2Br]^+$/BrACN in DMSO (Figure S11), which are qualitatively similar.

Analysis of Kinetic Parameters. A full summary of the values determined for the forward and reverse ATRP and OMRP reactions and their associated equilibrium constants appear in Table 2. The present study comprised two activator complexes ($[CuL^1]^+$ and $[CuL^2]^+$), two initiators (EBriB and BrACN), and two solvents (MeCN and DMSO). These 8 combinations showed that each of these three variables is important, and any variations in K_{ATRP} (k_{act}/k_{deact}) should be carefully compared. The tertiary radical of EBriB ($Me_2C^\bullet COOEt$) was unable to form an organocopper(II) complex, while $[CuL^n(CH_2CN)]^+$ (n = 1, 2) complexes are formed rapidly due to a relief of steric bulk with the sterically unencumbered primary radical $NCCH_2^\bullet$. Similar features were noted with computational chemistry of related $[Cu(Me_6tren)]^+$ systems.[25] One striking feature is the solvent dependence of the formation of $[CuL^n(CH_2CN)]^+$ (n = 1, 2), which was an order of magnitude faster in MeCN than DMSO, but rapid in all cases. Rapid radical capture is necessary if the OMRP reaction is to be competitive with bimolecular radical dimerization (termination), which is typically also very fast (k_t = 10^9 M^{-1} s^{-1}). The $[CuL^n(CH_2CN)]^{+/0}$ redox response is reversible in both MeCN and DMSO which indicates the organocopper complexes are quite stable on the CV time scale, which is an emerging feature in the nascent chemistry of these unusual complexes.[24−26]

The values of k_{act} and k_{deact} show interesting dependences on Cu complex and solvent. The most apparent contrast is that k_{deact} is about an order of magnitude greater in DMSO than in MeCN, while k_{act} does not change markedly. Overall the K_{ATRP} values show that $[CuL^1]^+$, as yet untested, should be an equally effective ATRP catalyst as $[CuL^2]^+$/EBriB. This is despite the presence of NH groups as donor atoms, which have been essentially neglected to date as ATRP catalysts. The lower $[CuL^1Br]^{2+/+}$ redox potential compared to $[CuL^2Br]^{2+/+}$ does not lead to a significantly larger value of log K_{ATRP}, as variations to both k_{act} and k_{deact}, measured independently, result in some cancellation effects.

The cathodic currents of both redox couples increased with the concentration of BrACN in both MeCN and DMSO. The magnitude of this increase was significantly greater for the $[CuL^n(CH_2CN)]^{+/0}$ response below −800 mV, indicating that $[CuL^n(CH_2CN)]^+$ was being formed at the expense of $[CuL^nBr]^+$.

CONCLUSIONS

The effects of ligand structure, solvent, and alkyl halide initiator on ATRP activity were examined. The three complexes $[CuL^1Br]^+$, $[CuL^2Br]^+$, and $[CuL^3Br]^+$ were studied in both MeCN and DMSO, using EBriB and BrACN as initiators. $[CuL^1Br]^+$ and $[CuL^2Br]^+$ were both electrocatalytically active in generating radicals, while $[CuL^3Br]^+$ was not, presumably due to high $Cu^{II/I}$ redox potentials and irreversible electron transfer which suggested significant rearrangement upon reduction. Simulations of the CV data from $[CuL^1Br]^+$ and $[CuL^2Br]^+$ gave values for the equilibrium and rate constants associated with radical activation/deactivation and hence K_{ATRP}. In addition, the sterically unencumbered $NCCH_2^\bullet$ radical was shown to react rapidly with $[CuL^n]^+$ to generate the corresponding $[CuL^n(CH_2CN)]^+$ complexes in both MeCN and DMSO.

To date, Cu complexes of exclusively tertiary amine and pyridyl N-donors dominate ATRP catalysis. The present finding that $[CuL^1Br]^+$, despite bearing two secondary amines, exhibits comparable activity to the highly active tertiary amine

https://doi.org/10.1021/acs.inorgchem.1c01001
Inorg. Chem. 2021, 60, 9709−9719

$[CuL^2Br]^+$ is novel. As expected, this structural change lowered the redox potential of $[CuL^1Br]^{+/0}$ by about 100 mV relative to the tertiary amine analog $[CuL^2Br]^+$. The fact that radical activation was still rapid and unaffected by the secondary amine NH groups bodes well for the use of $[CuL^1Br]^+$ in ATRP in future studies and indicates that the NH groups are tolerant of radical formation.

■ ASSOCIATED CONTENT

Supporting Information

The Supporting Information is available free of charge at https://pubs.acs.org/doi/10.1021/acs.inorgchem.1c01001.

Additional figures and tables (PDF)

Accession Codes

CCDC 2074222 contains the supplementary crystallographic data for this paper. These data can be obtained free of charge via www.ccdc.cam.ac.uk/data_request/cif, or by emailing data_request@ccdc.cam.ac.uk, or by contacting The Cambridge Crystallographic Data Centre, 12 Union Road, Cambridge CB2 1EZ, UK; fax: +44 1223 336033.

■ AUTHOR INFORMATION

Corresponding Author

Paul V. Bernhardt − *School of Chemistry and Molecular Biosciences, University of Queensland, Brisbane 4072, Australia;* orcid.org/0000-0001-6839-1763; Email: p.bernhardt@uq.edu.au

Author

Jamie N. Melville − *School of Chemistry and Molecular Biosciences, University of Queensland, Brisbane 4072, Australia*

Complete contact information is available at: https://pubs.acs.org/10.1021/acs.inorgchem.1c01001

Notes

The authors declare no competing financial interest.

■ ACKNOWLEDGMENTS

We gratefully acknowledge financial support from the Australian Research Council (DP210102150).

■ REFERENCES

(1) Wang, J.-S.; Matyjaszewski, K. Controlled/"living" radical polymerization. atom transfer radical polymerization in the presence of transition-metal complexes. *J. Am. Chem. Soc.* **1995**, *117*, 5614−5615.

(2) Wang, J.-S.; Matyjaszewski, K. Controlled/"Living" Radical Polymerization. Halogen Atom Transfer Radical Polymerization Promoted by a Cu(I)/Cu(II) Redox Process. *Macromolecules* **1995**, *28*, 7901−7910.

(3) Braunecker, W. A.; Matyjaszewski, K. Controlled/living radical polymerization: Features, developments, and perspectives. *Prog. Polym. Sci.* **2007**, *32*, 93−146.

(4) Zerk, T. J.; Bernhardt, P. V. Redox-coupled structural changes in copper chemistry: Implications for atom transfer catalysis. *Coord. Chem. Rev.* **2018**, *375*, 173−190.

(5) Di Lena, F.; Matyjaszewski, K. Transition metal catalysts for controlled radical polymerization. *Prog. Polym. Sci.* **2010**, *35*, 959−1021.

(6) Braunecker, W.; Tsarevsky, N.; Gennaro, A.; Matyjaszewski, K. Thermodynamic Components of the Atom Transfer Radical Polymerization Equilibrium: Quantifying Solvent Effects. *Macromolecules* **2009**, *42*, 6348−6360.

(7) Matyjaszewski, K. Atom Transfer Radical Polymerization (ATRP): Current Status and Future Perspectives. *Macromolecules* **2012**, *45*, 4015−4039.

(8) Ribelli, T. G.; Fantin, M.; Daran, J.-C.; Augustine, K. F.; Poli, R.; Matyjaszewski, K. Synthesis and Characterization of the Most Active Copper ATRP Catalyst Based on Tris(4-dimethylaminopyridyl)-methylamine. *J. Am. Chem. Soc.* **2018**, *140*, 1525.

(9) Kwak, Y.; Magenau, A. J. D.; Matyjaszewski, K. ARGET ATRP of Methyl Acrylate with Inexpensive Ligands and ppm Concentrations of Catalyst. *Macromolecules* **2011**, *44*, 811−819.

(10) Mendonça, P. V.; Ribeiro, J. P. M.; Abreu, C. M. R.; Guliashvili, T.; Serra, A. C.; Coelho, J. F. J. Thiourea Dioxide As a Green and Affordable Reducing Agent for the ARGET ATRP of Acrylates, Methacrylates, Styrene, Acrylonitrile, and Vinyl Chloride. *ACS Macro Lett.* **2019**, *8*, 315−319.

(11) De Bon, F.; Ribeiro, D. C. M.; Abreu, C. M. R.; Rebelo, R. A. C.; Isse, A. A.; Serra, A. C.; Gennaro, A.; Matyjaszewski, K.; Coelho, J. F. J. Under pressure: electrochemically-mediated atom transfer radical polymerization of vinyl chloride. *Polym. Chem.* **2020**, *11*, 6745−6762.

(12) Bernhardt, P. V. On the structure, electrochemistry, and spectroscopy of the (N,N'-bis(2'-(dimethylamino)ethyl)-N,N'-dimethylpropane-1,3-diamine)copper(II) ion. *J. Am. Chem. Soc.* **1997**, *119*, 771.

(13) Sakurai, T.; Kimura, M.; Nakahara, A. A Facile Reduction of Copper(II) Leading to Formation of Stable Copper(I) Complexes. Redox Properties of Four- and Five-coordinate Copper Complexes. *Bull. Chem. Soc. Jpn.* **1981**, *54*, 2976−2978.

(14) Nikles, D. E.; Powers, M. J.; Urbach, F. L. Copper(II) complexes with tetradentate bis(pyridyl)-dithioether and bis(pyridyl)-diamine ligands. Effect of thio ether donors on the electronic absorption spectra, redox behavior, and EPR parameters of copper(II) complexes. *Inorg. Chem.* **1983**, *22*, 3210−3217.

(15) Rybak-Akimova, E. V.; Nazarenko, A. Y.; Chen, L.; Krieger, P. W.; Herrera, A. M.; Tarasov, V. V.; Robinson, P. D. Synthesis, characterization, redox properties, and representative X-ray structures of four- and five-coordinate copper(II) complexes with polydentate aminopyridine ligands. *Inorg. Chim. Acta* **2001**, *324*, 1−15.

(16) Hartman, J. R.; Vachet, R. W.; Pearson, W.; Wheat, R. J.; Callahan, J. H. A comparison of the gas, solution, and solid state coordination environments for the copper(II) complexes of a series of aminopyridine ligands of varying coordination number. *Inorg. Chim. Acta* **2003**, *343*, 119−132.

(17) Hartman, J. R.; Kammier, A. L.; Spracklin, R. J.; Pearson, W. H.; Combariza, M. Y.; Vachet, R. W. A comparison of the gas, solution, and solid state coordination environments for the Cu(II) complexes of a series of linear aminopyridine ligands with varying ratios of 5- and 6-membered chelate rings. *Inorg. Chim. Acta* **2004**, *357*, 1141−1151.

(18) Kumar, P.; Kalita, A.; Mondal, B. Nitric oxide reactivity of Cu(II) complexes of tetra- and pentadentate ligands: structural influence in deciding the reduction pathway. *Dalton Trans.* **2013**, *42*, 5731−5739.

(19) Pandiyan, T.; Guadalupe, H. J.; Cruz, J.; Bernès, S.; Ugalde-Salvdivar, V. M.; González, I. DFT and Experimental Studies of Perchlorate Ion Coordination in cis/trans -Copper(II) Complexes of Tetradentate Pyridyl Ligands. *Eur. J. Inorg. Chem.* **2008**, *2008*, 3274−3285.

(20) Tang, W.; Kwak, Y.; Braunecker, W.; Tsarevsky, N. V.; Coote, M. L.; Matyjaszewski, K. Understanding atom transfer radical polymerization: effect of ligand and initiator structures on the equilibrium constants. *J. Am. Chem. Soc.* **2008**, *130*, 10702−10713.

(21) Bell, C. A.; Bernhardt, P. V.; Monteiro, M. J. A rapid electrochemical method for determining rate coefficients for copper-catalyzed polymerizations. *J. Am. Chem. Soc.* **2011**, *133*, 11944−11947.

(22) Zerk, T. J.; Bernhardt, P. V. Solvent dependent anion dissociation limits copper(I) catalysed atom transfer reactions. *Dalton Trans.* **2013**, *42*, 11683−11694.

(23) Zerk, T. J.; Bernhardt, P. V. New Method for Exploring Deactivation Kinetics in Copper-Catalyzed Atom-Transfer-Radical Reactions. *Inorg. Chem.* **2014**, *53*, 11351−11353.
(24) Zerk, T. J.; Bernhardt, P. V. Organo-Copper(II) Complexes as Products of Radical Atom Transfer. *Inorg. Chem.* **2017**, *56*, 5784−5792.
(25) Zerk, T. J.; Gahan, L. R.; Krenske, E. H.; Bernhardt, P. V. The fate of copper catalysts in atom transfer radical chemistry. *Polym. Chem.* **2019**, *10*, 1460−1470.
(26) Fantin, M.; Lorandi, F.; Ribelli, T.; Szczepaniak, G.; Enciso, A. E.; Fliedel, C.; Thevenin, L.; Isse, A. A.; Poli, R.; Matyjaszewski, K. Impact of Organometallic Intermediates on Copper-Catalyzed Atom Transfer Radical Polymerization. *Macromolecules* **2019**, *52*, 4079−4090.
(27) Fantin, M.; Isse, A. A.; Bortolamei, N.; Matyjaszewski, K.; Gennaro, A. Electrochemical approaches to the determination of rate constants for the activation step in atom transfer radical polymerization. *Electrochim. Acta* **2016**, *222*, 393−401.
(28) Ribelli, T. G.; Wahidur Rahaman, S. M.; Daran, J. C.; Krys, P.; Matyjaszewski, K.; Poli, R. Effect of Ligand Structure on the Cu^{II}-R OMRP Dormant Species and Its Consequences for Catalytic Radical Termination in ATRP. *Macromolecules* **2016**, *49*, 7749−7757.
(29) Poli, R. Relationship between one-electron transition-metal reactivity and radical polymerization processes. *Angew. Chem., Int. Ed.* **2006**, *45*, 5058−5070.
(30) Lorenz, S.; Plietker, B. Selectivity Trends in Olefin Epoxidations Catalyzed by (NNNN)Manganese(+II) Complexes using Trifluoroethanol as the Solvent. *ChemCatChem* **2016**, *8*, 3203−3206.
(31) Rudolph, M.; Feldberg, S. W. *DigiSim*; Bioanalytical Systems: West Lafayette, 2004.
(32) Maeder, M.; King, P. *ReactLab EQUILIBRIA*, 1.1; JPlus Consulting Pty. Ltd.: Western Australia, 2010.
(33) Sheldrick, G. M. A short history of SHELX. *Acta Crystallogr., Sect. A: Found. Crystallogr.* **2008**, *64*, 112−122.
(34) Farrugia, L. J. WinGX suite for small-molecule single-crystal crystallography. *J. Appl. Crystallogr.* **1999**, *32*, 837−838.
(35) Macrae, C. F.; Bruno, I. J.; Chisholm, J. A.; Edgington, P. R.; McCabe, P.; Pidcock, E.; Rodriguez-Monge, L.; Taylor, R.; Van De Streek, J.; Wood, P. A. Mercury CSD 2.0 − new features for the visualization and investigation of crystal structures. *J. Appl. Crystallogr.* **2008**, *41*, 466−470.
(36) Xu, L.; Pierreroy, J.; Patrick, B. O.; Orvig, C. Chemistry of Re with N,N′-Bis(2-pyridylmethyl)ethylenediamine (H2pmen): Hydrolysis, Dehydrogenation, and Ternary Complexes. *Inorg. Chem.* **2001**, *40*, 2005−2010.
(37) Drew, M. G. B.; Foreman, M. R. S.; Hudson, M. J.; Kennedy, K. F. Structural studies of lanthanide complexes with tetradentate nitrogen ligands. *Inorg. Chim. Acta* **2004**, *357*, 4102−4112.
(38) Hashemi, L.; Morsali, A. Sonochemical synthesis of nanostructured lead(II) complex: precursor for the preparation of PbO nano-structures. *J. Coord. Chem.* **2011**, *64*, 4088−4097.
(39) Chandrasekhar, V.; Hajra, T.; Bera, J. K.; Rahaman, S. M. W.; Satumtira, N.; Elbjeirami, O.; Omary, M. A. Ligand-Bridged Dinuclear Cyclometalated Ir^{III} Complexes: From Metallamacrocycles to Discrete Dimers. *Inorg. Chem.* **2012**, *51*, 1319−1329.
(40) Ebralidze, I. I.; Leitus, G.; Shimon, L. J. W.; Wang, Y.; Shaik, S.; Neumann, R. Structural variability in manganese(II) complexes of N,N′-bis(2-pyridinylmethylene) ethane (and propane) diamine ligands. *Inorg. Chim. Acta* **2009**, *362*, 4713−4720.
(41) Sun, O.; Chen, P.; Li, H.-F.; Gao, T.; Sun, W.-B.; Li, G.-M.; Yan, P.-F. A series of dinuclear lanthanide(III) complexes constructed from Schiff base and β-diketonate ligands: synthesis, structure, luminescence and SMM behavior. *CrystEngComm* **2016**, *18*, 4627−4635.
(42) Pal, P. K.; Chowdhury, S.; Purkayastha, P.; Tocher, D. A.; Datta, D. A novel double-stranded dinuclear copper(I) helicate having a photoluminescent CuI_2N_8 chromophore. *Inorg. Chem. Commun.* **2000**, *3*, 585−589.
(43) Zhou, X.-H.; Wu, T.; Li, D. Structural variations and spectroscopic properties of copper(I) complexes with bis(schiff base) ligands. *Inorg. Chim. Acta* **2006**, *359*, 1442−1448.
(44) Díaz, D. E.; Llanos, L.; Arce, P.; Lorca, R.; Guerrero, J.; Costamagna, J.; Aravena, D.; Ferraudi, G.; Oliver, A.; Lappin, A. G.; Lemus, L. Steric and Electronic Factors Affecting the Conformation of Bimetallic Cu^{I} Complexes: Effect of the Aliphatic Spacer of Tetracoordinating Schiff-Base Ligands. *Chem. - Eur. J.* **2018**, *24*, 13839−13849.
(45) Addison, A. W.; Rao, T. N.; Reedijk, J.; van Rijn, J.; Verschoor, G. C. Synthesis, structure, and spectroscopic properties of copper(II) compounds containing nitrogen−sulphur donor ligands; the crystal and molecular structure of aqua[1,7-bis(N-methylbenzimidazol-2′-yl)-2,6-dithiaheptane]copper(II) perchlorate. *J. Chem. Soc., Dalton Trans.* **1984**, 1349−1356.
(46) Blackman, A. G.; Schenk, E. B.; Jelley, R. E.; Krenske, E. H.; Gahan, L. R. Five-coordinate transition metal complexes and the value of τ5: observations and caveats. *Dalton Trans.* **2020**, *49*, 14798−14806.
(47) Alvarez, S.; Llunell, M. Continuous symmetry measures of penta-coordinate molecules: Berry and non-Berry distortions of the trigonal bipyramid. *J. Chem. Soc., Dalton Trans.* **2000**, 3288−3303.
(48) Khosrowabadi Kotyk, J. F.; Ziller, J. W.; Yang, J. Y. Copper tetradentate N2Py2 complexes with pendant bases in the secondary coordination sphere: improved ligand synthesis and protonation studies. *J. Coord. Chem.* **2016**, *69*, 1990−2002.
(49) Mautner, F. A.; Koikawa, M.; Mikuriya, M.; Harrelson, E. V.; Massoud, S. S. Copper(II)−azido complexes constructed from polypyridyl amine ligands. *Polyhedron* **2013**, *59*, 17−22.
(50) Bailey, N. A.; McKenzie, E. D.; Worthington, J.; Crystal, M. and molecular structure of a solvate of chloro-[1,6-bis-(2'-pyridyl)-2,5-diazahexane]copper(II) chloride. *J. Chem. Soc., Dalton Trans.* **1973**, 1227.
(51) Kani, Y.; Ohba, S.; Kunita, M.; Nishida, Y. [1,6-Bis(2-pyridylmethyl)-2,5-diazahexane-κ(4)N]chlorocopper(II) perchlorate. *Acta Crystallogr., Sect. C: Cryst. Struct. Commun.* **2000**, *56*, E197−E197.
(52) Mautner, F. A.; Mikuriya, M.; Ishida, H.; Sakiyama, H.; Louka, F. R.; Humphrey, J. W.; Massoud, S. S. Dicyanamido-metal(II) complexes. Part 4: Synthesis, structure and magnetic characterization of polynuclear Cu(II) and Ni(II) complexes bridged by μ-1,5-dicyanamide. *Inorg. Chim. Acta* **2009**, *362*, 4073−4080.
(53) Shen, J.; Wang, M.; Gao, J.; Han, H.; Liu, H.; Sun, L. Improvement of Electrochemical Water Oxidation by Fine-Tuning the Structure of Tetradentate N4 Ligands of Molecular Copper Catalysts. *ChemSusChem* **2017**, *10*, 4581−4588.
(54) Glerup, J.; Goodson, P. A.; Hodgson, D. J.; Michelsen, K. Magnetic exchange through oxalate bridges: synthesis and characterization of (μ-oxalato)dimetal(II) complexes of manganese, iron, cobalt, nickel, copper, and zinc. *Inorg. Chem.* **1995**, *34*, 6255.

https://doi.org/10.1021/acs.inorgchem.1c01001
Inorg. Chem. 2021, 60, 9709−9719